

MERba: Multi-Receptive Field MambaVision for Micro-Expression Recognition

Xinglong Mao, Shifeng Liu, Sirui Zhao*, Tong Xu, and Enhong Chen*

State Key Laboratory of Cognitive Intelligence, University of Science and Technology of China

(* Corresponding authors)

maoxl@mail.ustc.edu.cn, {siruit,cheneh}@ustc.edu.cn

Abstract—Micro-expressions (MEs) are brief, involuntary facial movements that reveal genuine emotions, holding significant potential in psychological diagnosis and criminal investigations. Despite notable advances in automatic ME recognition (MER), existing methods still struggle to jointly capture localized muscle activations and global facial dependencies, both critical for recognizing subtle emotional cues. To tackle this challenge, we propose MERba, a novel multi-receptive field architecture tailored for MER. MERba introduces a series of Local-Global Feature Integration stages, where fine-grained motion features are first extracted by local extractors containing MambaVision Mixers within non-overlapping windows, and then global dependencies across these regions are modeled via lightweight self-attention layers. This hierarchical design enables a progressive transition from localized perception to holistic facial understanding. Furthermore, we introduce an asymmetric multi-scanning strategy to eliminate redundant scanning directions and enhance local spatial perception. To address the high inter-class similarity among negative MEs, we introduce a Dual-Granularity Classification Module that decouples the recognition process into a coarse-to-fine paradigm. Experiments on two benchmark MER datasets demonstrate that MERba outperforms existing methods, with ablation studies confirming the effectiveness of each proposed component.

Index Terms—Micro-expression Recognition, Multi-Receptive Field, Asymmetric Multi-Scanning, MambaVision

I. INTRODUCTION

Micro-expressions (MEs) are involuntary facial movements that reveal an individual’s genuine emotions and intentions, holding significant value in psychological research [1]. Unlike regular facial expressions, MEs are characterized by short duration (typically less than 0.5 seconds [2]), low intensity, and occurrence in localized facial regions. Recent advances in ME recognition (MER) have shown promise in fields such as criminal investigations and psychological diagnostics [3], [4]. With the rapid development of artificial intelligence, automatic MER has gained growing attention in the field of affective computing. To extract effective features from MEs, researchers have developed various sophisticated feature extractors based on Convolutional Neural Networks (CNNs) [5]–[7] and Vision Transformers (ViTs) [8]–[10]. While CNNs excel at capturing local features, they have limitations in modeling global dependencies, whereas ViTs handle global information well, but are

computationally expensive and require large amounts of data, often leading to severe overfitting in MER.

Recently, the Mamba architecture [11], based on State Space Models (SSMs) [12], has demonstrated outstanding performance across various computer vision tasks [13], [14], particularly favored for its efficient linear time complexity, strong contextual awareness, and simplified network structure. Building on this foundation, MambaVision [15] extends Mamba by integrating Transformer blocks, forming a hybrid structure that aims to balance computational efficiency with long-range spatial dependency modeling. However, directly applying MambaVision to MER tasks is suboptimal, which fails to focus sufficiently on localized facial regions where MEs typically manifest as isolated Action Units (AUs) [16] and neglects fine-grained inter-region dependencies. Indeed, our empirical results show that the baseline MambaVision model underperforms significantly on MER benchmarks, indicating its limited capacity to capture subtle, region-specific motion dynamics.

To tackle this challenge, we propose MERba, a multi-receptive field architecture specifically designed for MER, incorporating the strengths of Mamba and Transformer in a task-adaptive manner. Specifically, MERba integrates fine-grained feature extraction with global dependency modeling through multiple ME Local-Global Feature Integration (LGFI) Stages. In each LGFI stage, instead of scanning the entire image, we define multiple non-overlapping local windows, within which MERba local extractors containing MambaVision Mixers (Mixers) operate independently to extract detailed ME motion cues. Considering emotional muscle movements span multiple facial areas, we employ global self-attention blocks after local extractors, where even a few Transformer layers per stage are sufficient to effectively model dependencies across local windows. Moreover, stage-wise downsampling expands the receptive field progressively, enabling a hierarchical transition from localized perception to full-face understanding.

It is worth noting that reasonable scanning strategies are critical for enhancing Mamba’s performance on visual tasks, with existing methods often utilizing bi-directional or symmetric scanning directions to better capture spatial contiguity relationships [13], [14], [17], [18]. However, due to the fixed facial structure after alignment and the natural left-right symmetry of human faces, such strategies introduce redundancy

and computational overhead. To overcome these limitations, we propose an Asymmetric Multi-Scanning Strategy, which uses four asymmetric scanning directions that retain spatial diversity while minimizing unnecessary duplication.

Additionally, to address the fine-grained nature of emotion recognition, especially in distinguishing subtle negative emotions like anger and disgust, we introduce a Dual-Granularity Classification Module (DGCM). This module uses two parallel classification heads: a coarse classifier that determines emotional polarity (e.g., positive or negative) and a fine classifier that resolves more nuanced emotional categories. This coarse-to-fine paradigm improves the model’s discriminability and robustness, especially under the imbalanced conditions common in ME datasets.

Conclusively, our contributions are summarized as follows:

- We propose MERba, a multi-receptive field architecture for MER, which integrates local extractors based on MambaVision Mixers with global self-attention mechanisms, facilitating fine-grained movement learning and global dependency modeling.
- We design an asymmetric multi-scanning strategy to eliminate redundant scanning directions and enhance local spatial perception.
- We introduce a selectively activated Dual-Granularity Classification Module that enhances fine-grained emotion recognition via a coarse-to-fine classification paradigm.
- Our approach achieves state-of-the-art performance on multiple benchmark ME datasets, with ablation studies validating the effectiveness of each proposed component.

II. RELATED WORK

A. Automatic Micro-Expression Recognition

Early automatic MER methods primarily relied on hand-crafted features, such as LBP-TOP [19] and Bi-WOOF [20]. Although these methods achieved certain success, their performance was limited by the complexity of feature design and adaptability to data variations. With the rise of deep learning, many researchers turned to CNNs for ME feature extraction. Notably, Liong et al. [5] employed a shallow three-stream CNN structure to separately process features from optical flow and optical strain in three dimensions. MERSiamC3D [6] and ME-PLAN [21] both utilized 3D-CNNs for spatiotemporal feature extraction from ME frame sequences. Recently, ViTs have gained traction in MER. Zhang et al. [22] completely abandoned traditional CNNs, relying solely on ViTs and LSTMs to achieve superior performance. Wang et al. [10] proposed HTNet, which stacks multiple hierarchical Transformer layers for feature extraction at different scales. In contrast to these approaches, our method utilizes SSMs for local feature extraction, combined with self-attention mechanisms to integrate global dependencies, enabling comprehensive modeling of fine-grained ME features across multiple receptive fields.

B. Scanning in Mamba

To enhance the spatial perception of Mamba, many researchers have focused on the design of scanning methods.

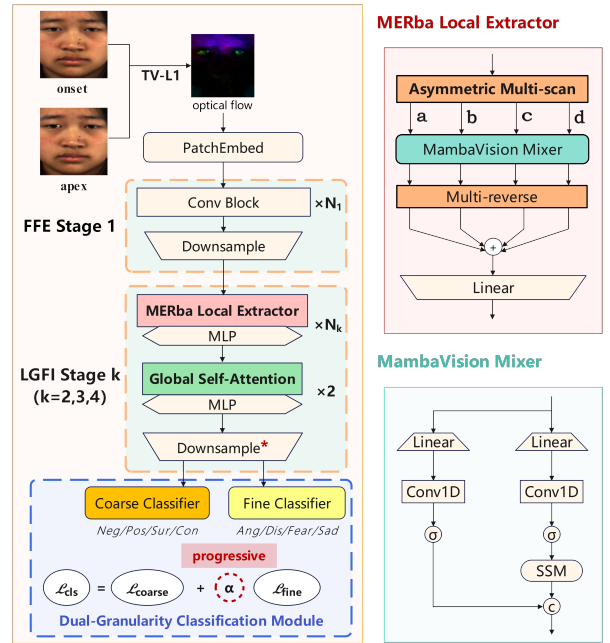


Fig. 1: The overall framework of MERba, with the specific structures of the MERba Local Extractor and MambaVision Mixer shown on the right side. * denotes that the Downsampling Layer in Stage 4 is replaced with 2D Batchnorm and 2D Average Pooling.

ViM [13] treated the image as 2D patch sequence and applied bi-directional scanning to capture global contextual information. VMamba [14] scanned bi-directionally along both horizontal and vertical axes, further enriching spatial information extraction. LocalMamba [17] not only performed bi-directional scanning globally but also within small local windows, and customized the scanning direction for each layer. PlainMamba [18] used continuous 2D scanning, maintaining the spatial continuity of adjacent tokens when transitioning between rows or columns. In contrast to above mentioned representative scanning methods, the asymmetric scanning strategy proposed in this paper fully considers the inherent properties of the human face and effectively models spatial relationships for MER tasks while avoiding redundancy.

III. METHODOLOGY

The overall framework of MERba, as illustrated in Figure 1, primarily consists of one Fast Feature Extraction (FFE) Stage and three Local-Global Feature Integration (LGFI) Stages. Specifically, we use TV-L1 [23] optical flow extracted from the onset and apex frames of ME sequences as input, denoted as $\mathbf{x}^{OF} = (u, v, m)^T \in \mathbb{R}^{H \times W \times 3}$, where u and v represent the horizontal and vertical components, respectively, and $m = \sqrt{u^2 + v^2}$. \mathbf{x}^{OF} is first tokenized into non-overlapping patches and projected into a higher-dimensional embedding space via a convolutional patch embedding layer. After patch embedding, initial feature extraction is performed through N_1 CNN layers of FFE Stage 1, consistent with MambaVision-B [15]. Then features progress through LGFI Stages 2, 3, and 4, each designed with different receptive fields (Section III-A). Within these stages, MERba local extractors employ an asymmetric

TABLE I: The detailed parameters setting of each stage in MERba. Stage 1 is a FFE stage and Stage 2, 3, 4 are LGFI stages.

	Block	Depth	Window Size	Input Size	Output Size
Patch Embed	Conv	-	-	$224 \times 224 \times 3$	$56 \times 56 \times 128$
Stage 1	Conv	$N_1 = 3$	-	$56 \times 56 \times 128$	$28 \times 28 \times 256$
Stage 2	MERba Local Extractor	$N_2 = 2$	7×7	$28 \times 28 \times 256$	$14 \times 14 \times 512$
	Global Self-attention	2	28×28		
Stage 3	MERba Local Extractor	$N_3 = 6$	7×7	$14 \times 14 \times 512$	$7 \times 7 \times 1024$
	Global Self-attention	2	14×14		
Stage 4	MERba Local Extractor	$N_4 = 4$	7×7	$7 \times 7 \times 1024$	$1 \times 1 \times 1024$
	Global Self-attention	2	7×7		

multi-scanning strategy (Section III-B) to enhance local spatial perception. Finally, when fine-grained recognition is required, classification is performed via the Dual-Granularity Classification Module (Section III-C), comprising parallel linear heads for coarse and fine emotional granularity.

A. Multi-Receptive Local-Global Feature Integration Stages

To effectively extract local motion features at different scales from ME samples, while simultaneously modeling global dependencies among different local regions within each scale, we propose the LGFI stages. These stages are applied as the second to fourth stages of the proposed MERba model.

1) *Multi-Receptive Field Feature Extraction*: Differing from the Mixer and Self-Attention hybrid architecture used in the original MambaVision, at each LGFI stage k , the input feature map $\mathbf{x}_k^{in} \in \mathbb{R}^{H_k \times W_k \times D_k}$ is divided into S_k non-overlapping local windows $\mathbf{w}_k^{(i)} \in \mathbb{R}^{w_H \times w_W \times D_k}$, where $i \in \{1, 2, \dots, S_k\}$. The number of windows is calculated as:

$$S_k = \frac{H_k \cdot W_k}{w_H \cdot w_W}, \quad (1)$$

where H_k and W_k represent the spatial height and width of the feature map at stage k , while D_k is the channel dimension. Notably, the window size is fixed across all LGFI stages, with $w_H = w_W = 7$.

Through the downsampling operations between stages, the spatial resolution of the feature map is halved at each subsequent stage, effectively increasing the receptive field of each local window. By the fourth stage, the local window size encompasses the entire feature map, allowing global feature extraction. This progression enables a transition from fine-grained local motion feature learning to a comprehensive global understanding of facial features. Table I provides the detailed parameter configurations for each stage in MERba.

2) *Localized ME Movement Learning*: Within each local window $\mathbf{w}_k^{(i)}$ at stage k , fine-grained motion features are extracted independently using N_k MERba local extractor blocks, each followed by MLP blocks. The extraction process leverages our asymmetric multi-scanning strategy, which applies four distinct scanning directions in parallel to capture diverse spatial contiguity relationships.

First, the spatial arrangement of each local window $\mathbf{w}_k^{(i)}$ is rearranged into 1D sequences $\mathbf{s}_k^{(i,s)} \in \mathbb{R}^{T_w \times D_k}$, where $T_w = w_H \cdot w_W$ and $s \in \{a, b, c, d\}$ represents each scanning direction. Each sequence is then processed by the Mixer block to extract local spatial features. The Mixer we used is the same

as MambaVision, but we have moved the last Linear layer to the end of our local extractor, as shown in Figure 1. The Mixer operation can be formulated as:

$$\mathbf{z}_k^{(i,s)} = \text{MixerBlock}(\mathbf{s}_k^{(i,s)}), \quad (2)$$

where $\mathbf{z}_k^{(i,s)} \in \mathbb{R}^{T_w \times D_k}$ denotes the intermediate representation of the sequence. Subsequently, the sequences are reversed to their original spatial arrangement, reconstructing the corresponding 2D feature maps $\mathbf{f}_k^{(i,s)} \in \mathbb{R}^{w_H \times w_W \times D_k}$. The four reconstructed maps are then fused together as:

$$\mathbf{f}_k^{(i)} = \sum_{s \in \{a, b, c, d\}} \mathbf{f}_k^{(i,s)}. \quad (3)$$

The fused feature map $\mathbf{f}_k^{(i)}$ is further refined by a Linear layer and a MLP block, producing the final localized feature representation for each local window $\mathbf{y}_k^{(i)} \in \mathbb{R}^{w_H \times w_W \times D_k}$:

$$\mathbf{y}_k^{(i)} = \text{MLP}(\text{Linear}(\mathbf{f}_k^{(i)})). \quad (4)$$

3) *Global Dependency Modeling*: Once all local windows are processed, their features $\mathbf{y}_k^{(i)}$, $i \in \{1, 2, \dots, S_k\}$, are concatenated and spatially restructured back into the original order to form a complete feature map $\mathbf{x}_k^{local} \in \mathbb{R}^{H_k \times W_k \times D_k}$.

To capture global dependencies across the local windows, two blocks each comprising a Multi-Head Self-Attention (MHSA) layer followed by a MLP are applied to \mathbf{x}_k^{local} , resulting in the global ME feature map $\mathbf{x}_k^{global} \in \mathbb{R}^{H_k \times W_k \times D_k}$:

$$\mathbf{x}_k^{global} = \text{MLP}(\text{MHSA}(\mathbf{x}_k^{local})). \quad (5)$$

Next, \mathbf{x}_k^{global} undergoes a downsampling operation to reduce spatial resolution by half while doubling channel dimensions, yielding the final output feature map $\mathbf{x}_k^{out} \in \mathbb{R}^{\frac{H_k}{2} \times \frac{W_k}{2} \times 2D_k}$, which also serves as the input \mathbf{x}_{k+1}^{in} of the next stage $k+1$. Notably, for Stage 4, we apply 2D batch normalization and average pooling instead of further downsampling, resulting in $\mathbf{x}_4^{out} \in \mathbb{R}^{1 \times 1 \times D_4}$, where $D_4 = D_3$.

B. Asymmetric Multi-Scanning Strategy

Existing scanning strategies, when involving bi-directional or symmetric directions, often lead to redundancy applying to MER. Specifically, bi-directional scanning involves reversing the order of a 1D sequence, but the relative positional relationships between tokens remain unchanged. Symmetric scanning refers to two different scanning orders derived from the left-right symmetry of a 2D image. However, when scanning

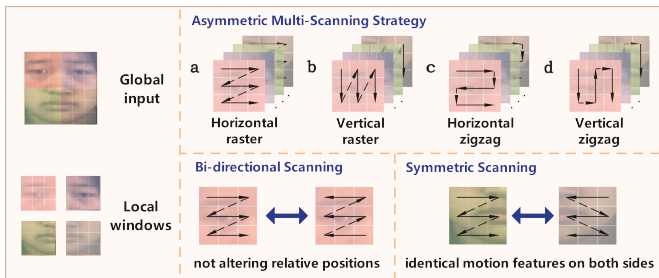


Fig. 2: Illustration of Asymmetric Multi-Scanning Strategy. The four scanning directions chosen in this strategy do not exhibit any bi-directional or symmetric relationships, effectively avoiding redundant scanning for human faces.

within a local window, the motion features obtained from the symmetrical left and right facial regions are identical.

Therefore, as shown in Figure 2, we employ four distinct scanning directions including **horizontal raster** (a), **vertical raster** (b), **horizontal zigzag** (c), and **vertical zigzag** (d) to process each local window $w_k^{(i)}$. Each scanning direction operates independently, starting at the top-left token of the window and proceeding according to its respective pattern:

- **Raster Scanning:** The sequence moves row-by-row (horizontally) or column-by-column (vertically), resetting to the start of the next row or column when switching.
- **Zigzag Scanning:** The sequence alternates directions within rows (horizontally) or columns (vertically), ensuring that adjacent tokens remain spatially close even during direction changes.

By combining these four complementary scanning directions, the strategy captures diverse spatial relationships and effectively models the subtle, localized motion features critical for MER. Importantly, this approach avoids the redundancy introduced by bi-directional or symmetric scanning, as each direction focuses on unique spatial dependencies.

C. Dual-Granularity Classification Module

We introduce DGCM to handle high inter-class similarity in MER. Specifically, unlike traditional approaches that rely on a single linear classification head with output dimension equal to the total number of emotion classes, DGCM adopts a coarse-to-fine classification paradigm via two parallel linear classifiers: a coarse-grained head h_{coarse} and a fine-grained head h_{fine} . h_{coarse} predicts the emotional polarity of the input ME sample among four broad categories: **negative**, **positive**, **surprise**, and **others (contempt)**. When a sample is predicted as **negative**, h_{fine} is activated to further disambiguate among four easily-confused negative emotions: **anger**, **disgust**, **fear**, and **sadness**.

During training, the outputs \hat{y}_{coarse} and \hat{y}_{fine} from both classification heads are used to compute two cross-entropy losses: $\mathcal{L}_{\text{coarse}}$ and $\mathcal{L}_{\text{fine}}$, respectively. The total training loss \mathcal{L}_{cls} is progressively weighted to balance learning dynamics:

$$\mathcal{L}_{\text{cls}} = 0.5 \cdot (\mathcal{L}_{\text{coarse}} + \alpha \cdot \mathcal{L}_{\text{fine}}), \quad (6)$$

TABLE II: Sample distribution of DFME-public dataset.¹

	Ang	Con	Dis	Fea	Hap	Sad	Sur	Total
Training	161	100	548	265	206	278	298	1856
Test A	39	34	129	62	63	46	101	474
Test B	41	37	58	38	42	35	48	299

¹ Ang-Anger, Con-Contempt, Dis-Disgust, Fea-Fear, Hap-Happiness, Sad-Sadness, Sur-Surprise.

TABLE III: Sample distribution of 3DB-Combined dataset.

	SMIC-HS	CASME II	SAMM	Combined
Negative	70	88	92	250
Positive	51	32	26	109
Surprise	43	25	15	83
Total	164	145	133	442

where the weighting factor α increases with training:

$$\alpha = \min\left(0.5 + \frac{2.0 \cdot \text{epoch}}{\text{total_epochs}}, 2.0\right). \quad (7)$$

Note that $\mathcal{L}_{\text{fine}}$ is computed only when the ground-truth label belongs to the negative emotion category.

At inference time, the final label \hat{y} is determined via:

- If the coarse prediction \hat{y}_{coarse} isn't **negative**, then \hat{y} is directly mapped from the coarse class to the original 7-class label space.
- Otherwise, the final label is derived from the fine prediction \hat{y}_{fine} through a predefined fine-to-full label mapping.

IV. EXPERIMENTS

In this section, we first provide an overview of the datasets and evaluation metrics used in our experiments. We then detail the implementation settings and present the results of our method. Finally, we conduct an ablation study to analyze the contributions of each component in our model.

A. Datasets and Evaluation Metrics

To ensure a comprehensive and fair comparison, we conducted experiments on two representative MER datasets, DFME-public (7 classes) and 3DB-Combined (3 classes). DFME-public refers to the publicly available portion of the DFME dataset [24], subject-independently divided into a fixed training set and two test sets. The model was trained using the entire training set and inference was conducted separately on Test A and Test B, using Unweighted F1-score (UF1), Unweighted Average Recall (UAR) and Accuracy (ACC) as evaluation metrics following [25]. For 3DB-Combined, which is a composite dataset of SMIC-HS [26], CASME II [27], and SAMM [28], we employed Leave-One-Subject-Out (LOSO) cross-validation with UF1 and UAR as evaluation metrics in line with MEGC2019 protocols [29]. Detailed sample distributions of both datasets are provided in Table II and III.

B. Implementation Settings

For all datasets, we first apply face detection, alignment, and cropping, following the same procedure as [24]. Subsequently, all images are resized to a uniform resolution of 224×224 . For the SMIC-HS dataset, which lacks apex frame labels, we employ the apex frame detection method from [21] to generate

TABLE IV: Comparison of experimental results with other methods on DFME-public dataset.

MER Methods	Test Set	UF1	UAR	ACC
FeatRef (2022) [7]	Test A	0.3410	0.3686	0.5084
Wang et al. (2024) [25]		0.4067	0.4074	0.4641
He et al. (2024) [25]		0.4123	0.4210	0.4873
HTNet ¹ (2024) [10]		0.3736	0.3821	0.4768
MambaVision-B ¹ (2024) [15]		0.4002	0.4064	0.4578
MERba-base² (ours)		0.4101	0.4123	0.4831
MERba-DGCM (ours)		0.4332	0.4287	0.5232
FeatRef (2022) [7]	Test B	0.2875	0.3228	0.3645
Wang et al. (2024) [25]		0.3534	0.3661	0.3813
He et al. (2024) [25]		0.4016	0.4008	0.4147
HTNet ¹ (2024) [10]		0.4076	0.4062	0.4214
MambaVision-B ¹ (2024) [15]		0.3929	0.3858	0.4080
MERba-base² (ours)		0.4114	0.4219	0.4415
MERba-DGCM (ours)		0.4302	0.4263	0.4415

¹ HTNet is reproduced using the hyperparameters reported in its original paper, and MambaVision-B is reproduced with the same hyperparameters as MERba-base.

² MERba-base denotes replacing DGCM with a single linear head which predicts all seven emotion categories.

the labels. During training, the only data augmentation applied is random horizontal flipping. The optimizer used is AdamW, with the learning rate warmed up over the first 5 epochs to $5e-4$, followed by a cosine decay scheduler, with a cooldown period over the last 10 epochs. The weight decay is set to 0.05, and the classification loss function is cross-entropy loss. The total number of training epochs is 200 for the DFME-public dataset. For the 3DB-combined dataset, the number of epochs per subject is 70. Early stopping is employed during training to prevent overfitting, and the dropout rate is set to 0.1. All experiments are conducted using the PyTorch framework, with training and inference performed on a single NVIDIA A100 Tensor Core GPU, and the training batch size is set to 128.

C. Experimental Results

1) *DFME-public dataset*: DFME-public test sets take FeatRef [7] as the baseline, and the results of top two teams are publicly available based on the official leaderboard [25]. We have also reproduced HTNet [10] and MambaVision-B [15] for a more comprehensive comparison. As shown in Table IV, on both Test Set A and B, MERba with DGCM outperforms all state-of-the-art (SOTA) methods, demonstrating superior performance in the challenging fine-grained 7-class MER task.

2) *3DB-Combined datasets*: The results are compared across a range of baseline methods, spanning hand-crafted [19], [20], 2D-CNN [5], [7], 3D-CNN [21], and Transformer-based [9], [10], [22] approaches. MambaVision-B [15] and our MERba represent the latest models using SSM+ViT backbones. As shown in Table V, our method achieves SOTA results on SMIC-HS, SAMM, and the 3DB-combined dataset. On CASME II, it performs on par with the best-performing method (HTNet), trailing by no more than 0.5% in both UF1 and UAR. Notably, on the SAMM dataset, which has a more diverse ethnic groups, our UF1 is 5.7% higher than that of HTNet. Overall, these results highlight the robustness and competitiveness of our approach.

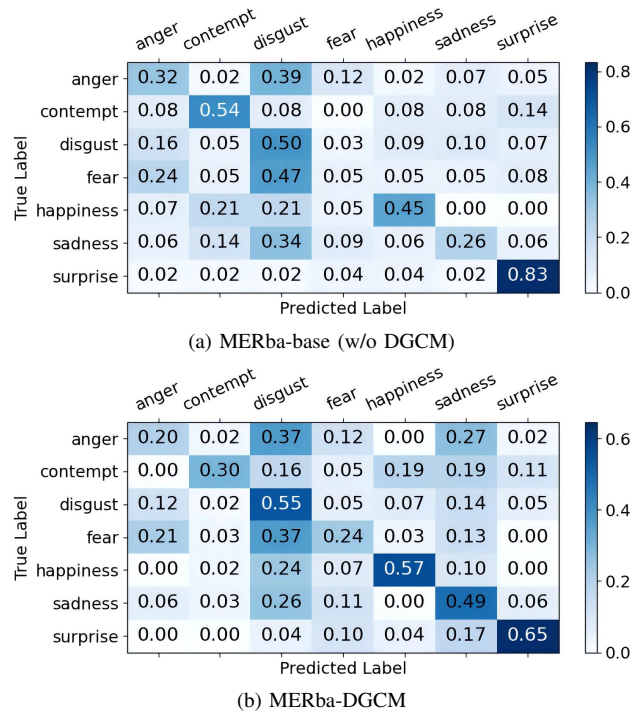


Fig. 3: Confusion Matrices on DFME-public Test B.

D. Ablation Study

1) *Local-Global Feature Integration*: We perform an ablation study to assess the effect of our proposed LGFI stages on the DFME-public Test B dataset, as shown in Table VI. On the one hand, when self-attention is applied only within the local window like the extractor, the model performs poorly, struggling to capture global dependencies between different facial regions during ME occurrences. On the other hand, when we discard the local window (i.e., both extractors and self-attention are applied to the entire feature map), the model achieves a UF1 of 0.3840 and a UAR of 0.3814. However, it still lacks the fine-grained spatial learning necessary for detecting subtle facial movements. The best performance is achieved by combining local extractors with global self-attention, demonstrating that associating local feature extraction with global dependency modeling provides a substantial improvement in MER performance.

2) *Asymmetric Multi-Scanning Strategy*: We first investigate the impact of the number of scanning directions on MER performance. As shown in Table VII, compared with using a single (a) or a pair of directions (a, b), introducing more scanning directions leads to consistent performance gains across UF1, UAR, and ACC. This confirms that incorporating diverse scanning combinations enhances the spatial perception capability of the local extractor in ME feature extraction. However, we also observe that adding bi-directional (a_{bi}, b_{bi}) or horizontal symmetric (a_{sy}, b_{sy}) counterparts to the base directions does not lead to significant improvements. In contrast, utilizing our proposed asymmetric multi-scanning directions (a, b, c, d) achieves the best performance, indicating its ability to capture the most discriminative motion patterns

TABLE V: Experimental results compared with state-of-the-art methods on 3DB-Combined.

MER Methods	Backbone	Combined		SMIC-HS		CASME II		SAMM	
		UF1	UAR	UF1	UAR	UF1	UAR	UF1	UAR
LBP-TOP (2014) [19]	Hand-crafted	0.5882	0.5785	0.2000	0.5280	0.7026	0.7429	0.3954	0.4102
Bi-WOOF (2018) [20]	Hand-crafted	0.6296	0.6227	0.5727	0.5829	0.7805	0.8026	0.5211	0.5139
STSTNet (2019) [5]	2D-CNN	0.7353	0.7605	0.6801	0.7013	0.8382	0.8686	0.6588	0.6810
FeatRef (2022) [7]	2D-CNN	0.7838	0.7832	0.7011	0.7083	0.8915	0.8873	0.7372	0.7155
ME-PLAN (2022) [21]	3D-CNN	0.7715	0.7864	0.7127	0.7256	0.8632	0.8778	0.7164	0.7418
SLSTT (2022) [22]	ViT+LSTM	0.8160	0.7900	0.7400	0.7200	0.9010	0.8850	0.7150	0.6430
MFDAN (2024) [9]	ViT	0.8453	0.8688	0.6815	0.7043	0.9134	0.9326	0.7871	0.8196
HTNet (2024) [10]	ViT	0.8603	0.8475	0.8049	0.7905	0.9532	0.9516	0.8131	0.8124
MambaVision-B ¹ (2024) [15]	SSM+ViT	0.8193	0.8227	0.7382	0.7435	0.9268	0.9327	0.7617	0.7520
MERba (ours)	SSM+ViT	0.8840	0.8777	0.8312	0.8309	0.9498	0.9470	0.8701	0.8423

¹ MambaVision-B is reproduced with the same parameters as MERba.

TABLE VI: Ablation study for Local-Global Feature Integration on DFME-public Test B.

Extractor	Self-Attention	UF1	UAR	ACC
local	local	0.3749	0.3637	0.3746
global	global	0.3840	0.3814	0.4013
local	global	0.4302	0.4263	0.4415

TABLE VII: Ablation study for Asymmetric Multi-Scanning on DFME-public Test B.

Directions ¹	UF1	UAR	ACC
<i>a</i>	0.3814	0.3713	0.3746
<i>a + b</i>	0.3849	0.3810	0.3946
<i>c + d</i>	0.3929	0.3939	0.4147
<i>a + a_{bi} + b + b_{bi}</i>	0.4102	0.4020	0.4147
<i>a + a_{sy} + b + b_{sy}</i>	0.4076	0.4051	0.4181
<i>a + b + c + d</i>	0.4302	0.4263	0.4415

¹ *a*, *b*, *c*, *d* are consistent with the corresponding direction in Figure 2. The subscripts "*bi*" or "*sy*" respectively represent the scanning directions exhibiting a bi-directional or horizontal symmetric relationship with the original direction *a* or *b*.

without introducing unnecessary directional overlap.

3) *Dual-Granularity Classification Module*: In Table II, we report the MER performance both with and without DGCM. It can be observed that introducing DGCM consistently improves performance on both DFME-public Test A and B, yielding UF1 gains of 2.31% and 1.88%, respectively. Furthermore, the confusion matrices in Figure 3 provide deeper insights into the impact of DGCM. Notably, the number of true positives for three *negative* emotions—*disgust*, *fear*, and *sadness*—increases significantly. In addition, the tendency to misjudge *fear* as *anger/disgust*, as well as the reciprocal confusion between *anger* and *disgust*, is noticeably alleviated. These observations confirm DGCM’s effectiveness in disambiguating fine-grained negative emotions. However, this improvement comes with a trade-off: accuracy for certain non-negative emotions such as *surprise* slightly decreases, possibly due to the model focusing more on subtle negative distinctions at the expense of broader category coverage.

V. CONCLUSION

In this paper, we proposed MERba, a novel architecture for MER, designed to address key challenges in feature extraction, global dependency modeling, and high inter-class similarity of MEs. By combining local extractors with global self-attention mechanisms, MERba effectively captures both fine-grained facial features and long-range dependencies, which are crucial for recognizing MEs. The asymmetric multi-scanning strategy reduces redundancy in scanning while enhancing the model’s

spatial perception. Additionally, DGCM introduces a dual-head coarse-to-fine paradigm that disentangles emotion polarity from subtle category distinctions, enhancing recognition of highly similar MEs. The experimental results on benchmark MER datasets DFME-public and 3DB-Combined demonstrate that MERba outperforms existing methods, setting new state-of-the-art performance.

REFERENCES

- Xianye Ben, Yi Ren, Junping Zhang, Su-Jing Wang, Kidiyo Kpalma, Weixiao Meng, and Yong-Jin Liu, "Video-based facial micro-expression analysis: A survey of datasets, features and algorithms," *IEEE transactions on pattern analysis and machine intelligence*, vol. 44, no. 9, pp. 5826–5846, 2021.
- Wen-Jing Yan, Qi Wu, Jing Liang, Yu-Hsin Chen, and Xiaolan Fu, "How fast are the leaked facial expressions: The duration of micro-expressions," *Journal of Nonverbal Behavior*, vol. 37, pp. 217–230, 2013.
- Paul Ekman, *Telling lies: Clues to deceit in the marketplace, politics, and marriage (revised edition)*, WW Norton & Company, 2009.
- Wei Huang, "Elderly depression recognition based on facial micro-expression extraction," *Traitement du Signal*, vol. 38, no. 4, 2021.
- Sze-Teng Liong, Yee Siang Gan, John See, Huai-Qian Khor, and Yen-Chang Huang, "Shallow triple stream three-dimensional cnn (ststnet) for micro-expression recognition," in *2019 14th IEEE international conference on automatic face & gesture recognition (FG 2019)*. IEEE, 2019, pp. 1–5.
- Sirui Zhao, Hanqing Tao, Yangsong Zhang, Tong Xu, Kun Zhang, Zhongkai Hao, and Enhong Chen, "A two-stage 3d cnn based learning method for spontaneous micro-expression recognition," *Neurocomputing*, vol. 448, pp. 276–289, 2021.
- Ling Zhou, Qirong Mao, Xiaohua Huang, Feifei Zhang, and Zhihong Zhang, "Feature refinement: An expression-specific feature learning and fusion method for micro-expression recognition," *Pattern Recognition*, vol. 122, pp. 108275, 2022.
- Mengting Wei, Wenming Zheng, Xingxun Jiang, Yuan Zong, Cheng Lu, and Jiateng Liu, "A novel magnification-robust network with sparse self-attention for micro-expression recognition," in *2022 26th International Conference on Pattern Recognition (ICPR)*. IEEE, 2022, pp. 1120–1126.
- Wenhao Cai, Junli Zhao, Ran Yi, Mingjing Yu, Fuqing Duan, Zhenkuan Pan, and Yong-Jin Liu, "Mfdan: Multi-level flow-driven attention network for micro-expression recognition," *IEEE Transactions on Circuits and Systems for Video Technology*, 2024.
- Zhifeng Wang, Kaihao Zhang, Wenhao Luo, and Ramesh Sankaranarayanan, "Htnet for micro-expression recognition," *Neurocomputing*, vol. 602, pp. 128196, 2024.
- Albert Gu and Tri Dao, "Mamba: Linear-time sequence modeling with selective state spaces," *arXiv preprint arXiv:2312.00752*, 2023.
- Rudolph Emil Kalman, "A new approach to linear filtering and prediction problems," 1960.
- Lianghui Zhu, Bencheng Liao, Qian Zhang, Xinlong Wang, Wenyu Liu, and Xinggong Wang, "Vision mamba: Efficient visual representation learning with bidirectional state space model," *arXiv preprint arXiv:2401.09417*, 2024.

- [14] Yue Liu, Yunjie Tian, Yuzhong Zhao, Hongtian Yu, Lingxi Xie, Yaowei Wang, Qixiang Ye, Jianbin Jiao, and Yunfan Liu, "Vmamba: Visual state space model," *Advances in neural information processing systems*, vol. 37, pp. 103031–103063, 2024.
- [15] Ali Hatamizadeh and Jan Kautz, "Mambavision: A hybrid mamba-transformer vision backbone," in *Proceedings of the Computer Vision and Pattern Recognition Conference*, 2025, pp. 25261–25270.
- [16] Paul Ekman and Wallace V Friesen, "Facial action coding system," *Environmental Psychology & Nonverbal Behavior*, 1978.
- [17] Tao Huang, Xiaohuan Pei, Shan You, Fei Wang, Chen Qian, and Chang Xu, "Localmamba: Visual state space model with windowed selective scan," in *European Conference on Computer Vision*. Springer, 2025, pp. 12–22.
- [18] Chenhongyi Yang, Zehui Chen, Miguel Espinosa, Linus Ericsson, Zhenyu Wang, Jiaming Liu, and Elliot J Crowley, "Plainmamba: Improving non-hierarchical mamba in visual recognition," *arXiv preprint arXiv:2403.17695*, 2024.
- [19] Guoying Zhao and Matti Pietikainen, "Dynamic texture recognition using local binary patterns with an application to facial expressions," *IEEE transactions on pattern analysis and machine intelligence*, vol. 29, no. 6, pp. 915–928, 2007.
- [20] Sze-Teng Liong, John See, KokSheik Wong, and Raphael C-W Phan, "Less is more: Micro-expression recognition from video using apex frame," *Signal Processing: Image Communication*, vol. 62, pp. 82–92, 2018.
- [21] Sirui Zhao, Huaying Tang, Shifeng Liu, Yangsong Zhang, Hao Wang, Tong Xu, Enhong Chen, and Cuntai Guan, "Me-plan: A deep prototypical learning with local attention network for dynamic micro-expression recognition," *Neural networks*, vol. 153, pp. 427–443, 2022.
- [22] Liangfei Zhang, Xiaopeng Hong, Ognjen Arandjelović, and Guoying Zhao, "Short and long range relation based spatio-temporal transformer for micro-expression recognition," *IEEE Transactions on Affective Computing*, vol. 13, no. 4, pp. 1973–1985, 2022.
- [23] Christopher Zach, Thomas Pock, and Horst Bischof, "A duality based approach for realtime tv-l 1 optical flow," in *Pattern Recognition: 29th DAGM Symposium, Heidelberg, Germany, September 12-14, 2007. Proceedings 29*. Springer, 2007, pp. 214–223.
- [24] Sirui Zhao, Huaying Tang, Xinglong Mao, Shifeng Liu, Yiming Zhang, Hao Wang, Tong Xu, and Enhong Chen, "Dfme: A new benchmark for dynamic facial micro-expression recognition," *IEEE Transactions on Affective Computing*, 2023.
- [25] Sirui Zhao, Huaying Tang, Xinglong Mao, and Shifeng Liu, "Dynamic micro-expression automatic recognition challenge on the fourth chinese conference on affective computing," <https://mea-lab-421.github.io/CCAC-page/>, July 10 2024.
- [26] Xiaobai Li, Tomas Pfister, Xiaohua Huang, Guoying Zhao, and Matti Pietikainen, "A spontaneous micro-expression database: Inducement, collection and baseline," in *2013 10th IEEE International Conference and Workshops on Automatic face and gesture recognition (fg)*. IEEE, 2013, pp. 1–6.
- [27] Wen-Jing Yan, Xiaobai Li, Su-Jing Wang, Guoying Zhao, Yong-Jin Liu, Yu-Hsin Chen, and Xiaolan Fu, "Casmie ii: An improved spontaneous micro-expression database and the baseline evaluation," *PLoS one*, vol. 9, no. 1, pp. e86041, 2014.
- [28] Adrian K Davison, Cliff Lansley, Nicholas Costen, Kevin Tan, and Moi Hoon Yap, "Samm: A spontaneous micro-facial movement dataset," *IEEE transactions on affective computing*, vol. 9, no. 1, pp. 116–129, 2016.
- [29] John See, Moi Hoon Yap, Jingting Li, Xiaopeng Hong, and Su-Jing Wang, "Megc 2019—the second facial micro-expressions grand challenge," in *2019 14th IEEE International Conference on Automatic Face & Gesture Recognition (FG 2019)*. IEEE, 2019, pp. 1–5.